

First-principles simulations of thermodynamical and structural properties of liquid Al_2O_3 under pressure

Ashok K. Verma,^{1,*} P. Modak,¹ and Bijaya B. Karki²¹*High Pressure and Synchrotron Radiation Physics Division, Bhabha Atomic Research Centre, Mumbai-400085, India*²*Department of Computer Science, Department of Geology and Geophysics, and Center for Computation and Technology, Louisiana State University, Baton Rouge, Louisiana 70803, USA*

(Received 8 July 2011; published 22 November 2011)

First-principles molecular dynamics simulations within local density approximation were carried out for liquid alumina over a pressure range from 0 to 150 GPa at 3000, 4000, and 6000 K. Liquid alumina is more compressible and less dense than solid alumina, and the density difference between two phases decreases with compression with a density crossover occurring around 90 GPa at 3000 K. The calculated thermodynamic properties including specific heat, thermal expansion coefficient, and Grüneisen parameter are strongly pressure dependent. The liquid structure is more sensitive to compression than temperature: mean Al–O and O–Al coordination numbers which remain nearly unchanged on isochoric heating increase from 5.2 and 3.4, respectively, at 0 GPa to 6.8 and 4.5, respectively, at 150 GPa along 3000 K isotherm. Coordination environments consist of various species with low-coordination species (three- and four-coordinated Al atoms) disappearing and high-coordination species (six- and seven-coordinated Al atoms) appearing as the liquid is compressed. We also analyze the structure in terms of bond distances and bond angles.

DOI: [10.1103/PhysRevB.84.174116](https://doi.org/10.1103/PhysRevB.84.174116)

PACS number(s): 61.20.Ja, 65.20.–w, 62.50.–p, 71.15.Mb

I. INTRODUCTION

Alumina (Al_2O_3) is one of the most important refractory ceramic oxides used in numerous applications such as cutting tools, electronic devices, optics, biomedical, mechanical engineering, and high pressure experiments. In addition to its technological importance, alumina is also considered to be an important component in any Earth's mantle compositional model. In particular, knowledge about molten Al_2O_3 at high pressure is essential to understanding the properties of geologically relevant silicate melts (magmas) and how they have been controlling the dynamics throughout the Earth's history.^{1–10}

Experimental studies of liquid alumina have provided important information about its structure.^{11,12} Most of the data on mean Al–O coordination fall in the range of 4–5 except the x-ray diffraction results (Ref. 13), which quote a value of 5.6. The nuclear magnetic resonance (NMR) investigations suggest that the liquid primarily consists of four-coordinated Al with an average coordination of 4.5.^{14,15} While numerous first-principles investigations have been reported for crystalline alumina,^{2–5} liquid alumina is yet to be studied from first principles. Previous molecular dynamics simulations are based on the model interaction potentials, which were fitted either to experimental data or to the forces and multipoles derived from density functional theory.^{6–10} Such potentials allow longer run times and bigger supercells but their accuracy is questionable, especially under varying conditions of temperature and pressure. In recent years, the first-principles molecular dynamics (FPMD) approach has been applied successfully to many liquids.^{16–20} In this paper, we report a FPMD study of the thermodynamical and structural properties of liquid Al_2O_3 over a wide range of pressure at three temperatures, 3000, 4000, and 6000 K.

II. DETAILS OF SIMULATIONS

The first-principles molecular dynamics simulation method used is based on the finite temperature local density functional

theory and the projector augmented wave method as implemented in the VASP package.^{21–23} The Al and O potentials were generated with $3s^2, 3p^1$ and $2s^2, 2p^4$ valence configurations, respectively. The plane wave energy cutoff was 600 eV for which the Pulay stresses are negligible. Only the Γ point was used in the Brillouin zone integration. Thermodynamic pressure was obtained by adding the ideal gas contribution to the “external pressure” calculated in VASP.

A series of equilibrium FPMD simulations were carried out using a cubic supercell containing 24 formula units (48 Al + 72 O) in the canonical ensemble (NVT) with periodic boundary conditions imposed. Temperature was controlled by Nosé thermostat²⁴ and the equations of motion were solved iteratively with a 1 fs time step using the interatomic forces obtained from the self-consistent electronic structure calculations. Initial liquid configuration was generated by melting α - Al_2O_3 constrained inside a cube at 10 000 K followed by an equilibration period of 10 ps. The molten sample was then quenched down isochorically to desired temperatures. The liquid state was confirmed by inspection of the calculated radial and bond-angle distribution functions and mean square displacement functions. Ensemble averages of pressure (P) and internal energy (E) were computed by applying the block average technique.²⁵ The uncertainties are $\sigma_P = 1.1$ GPa and $\sigma_E = 6.5$ kJ/mole. To test the effect of system size on liquid properties, simulations were repeated with a double-sized supercell (containing 108 Al and 162 O atoms), which produced pressure and internal energy within statistical uncertainties. Simulations were run for 10–50 ps depending upon temperature and volume (density) conditions.

III. RESULTS AND DISCUSSION

A. Thermodynamical properties

The calculated pressure-volume isotherms (Fig. 1, left) can be described accurately by the Mie-Grüneisen thermal

TABLE I. Birch-Murnaghan equation-of-state fit parameters for liquid (fourth-order) and crystalline (third-order) alumina. Density (ρ_0) and bulk modulus (K_0) are in g/cm^3 and GPa, respectively. Previous theoretical (Refs. 2 and 4) and experimental (Refs. 26–31) results are given for comparison.

| | Liquid, 3000 K | Solid, 0 K | Solid, 3000 K | Liquid | Solid |
|----------|----------------|------------|---------------|-------------------------|---|
| ρ_0 | 3.038 | 4.062 | 3.683 | $\rho_0^{3000\text{K}}$ | $\rho_0: 3.98^{\text{a,b}}$ |
| K_0 | 36.50 | 265 | 169 | 2.85 ^c | $K_0: 258,^{\text{d}} 262,^{\text{e}}$ |
| K'_0 | 9.27 | 3.84 | 4.40 | 2.74 ^f | 255 ^b 254 ^a |
| K''_0 | -1.280 | | | 2.70 ^g | $K'_0: 4.06,^{\text{d}} 3.79,^{\text{e}}$ |
| | | | | 2.41 ^h | 5.1, ^b 4.27 ^a |

^aReference 30.

^bReference 31.

^cReference 26.

^dReference 2.

^eReference 4.

^fReference 27.

^gReference 28.

^hReference 29.

equation of state:

$$P(V, T) = P(V, T_{\text{ref}}) + \Delta P_{\text{therm}}(V, T). \quad (1)$$

Here, the first term represents the reference isotherm fitted to a fourth-order Birch-Murnaghan equation of state with $T_{\text{ref}} = 3000$ K. The second term represents thermal pressure given by

$$\Delta P_{\text{therm}}(V, T) = \left(\frac{\partial P}{\partial T} \right)_V (T - T_{\text{ref}}) \equiv B(V)(T - T_{\text{ref}}), \quad (2)$$

where the thermal pressure coefficient is $B(V) = 16.384 - 0.2261V$.

The fit parameters are given in Table I. The predicted liquid density $3.038 \text{ g}/\text{cm}^3$ at ambient pressure is higher by a

few percent than the experimental data,²⁶ which are scattered between 2.41 and $2.74 \text{ g}/\text{cm}^3$ (see Table I).^{27–29} The density overestimation can be attributed to local density approximation used because of its well-known overbinding nature.

The pressure-volume isotherms of corundum were also calculated at 0, 2000, and 3000 K (Fig. 1, right). Unlike liquid, crystalline phase P - V isotherms show a good fit to the third-order Birch-Murnaghan equation of state with 0 K as a reference temperature. The fit parameters agree well with previous theoretical^{2,4} and experimental^{30,31} results (Table I). At ambient pressure, Al_2O_3 solid expands by 10% over the temperature range of 0–3000 K in good agreement with the previous theoretical³² and experimental results.³³ Our results show that the liquid phase is more compressible (~ 4.5 times at zero pressure) than the solid phase along the 3000 K

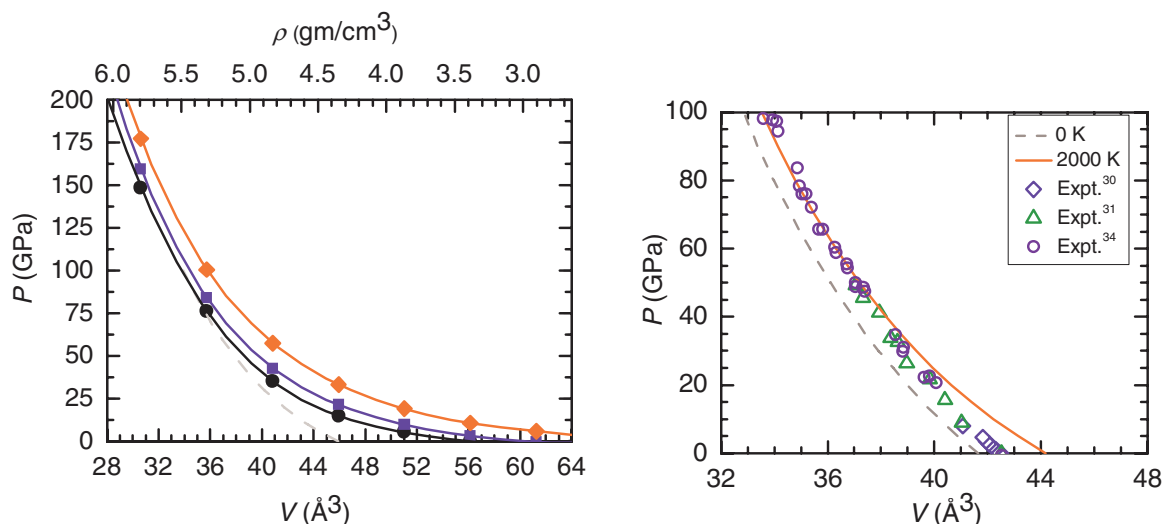


FIG. 1. (Color online) Pressure-volume relationships of liquid (left) and solid alumina (right). The calculated results are shown by circles (3000 K), squares (4000 K) and diamonds (6000 K) and smooth lines are fit to the Mie-Grüneisen equation of states. Dashed line shows solid isotherm at 3000 K (left). The experimental data at 300 K (Refs. 30 and 31) and the Hugoniot data for corundum from (Ref. 34) are shown for comparison. V is volume per formula unit. Note that Hugoniot represents curve in P - V - T space so as the Hugoniot pressure increases, temperature also increases causing thermal pressure to increase. This is why the Hugoniot data show a better match with 2000 K isotherm as pressure increases (right).

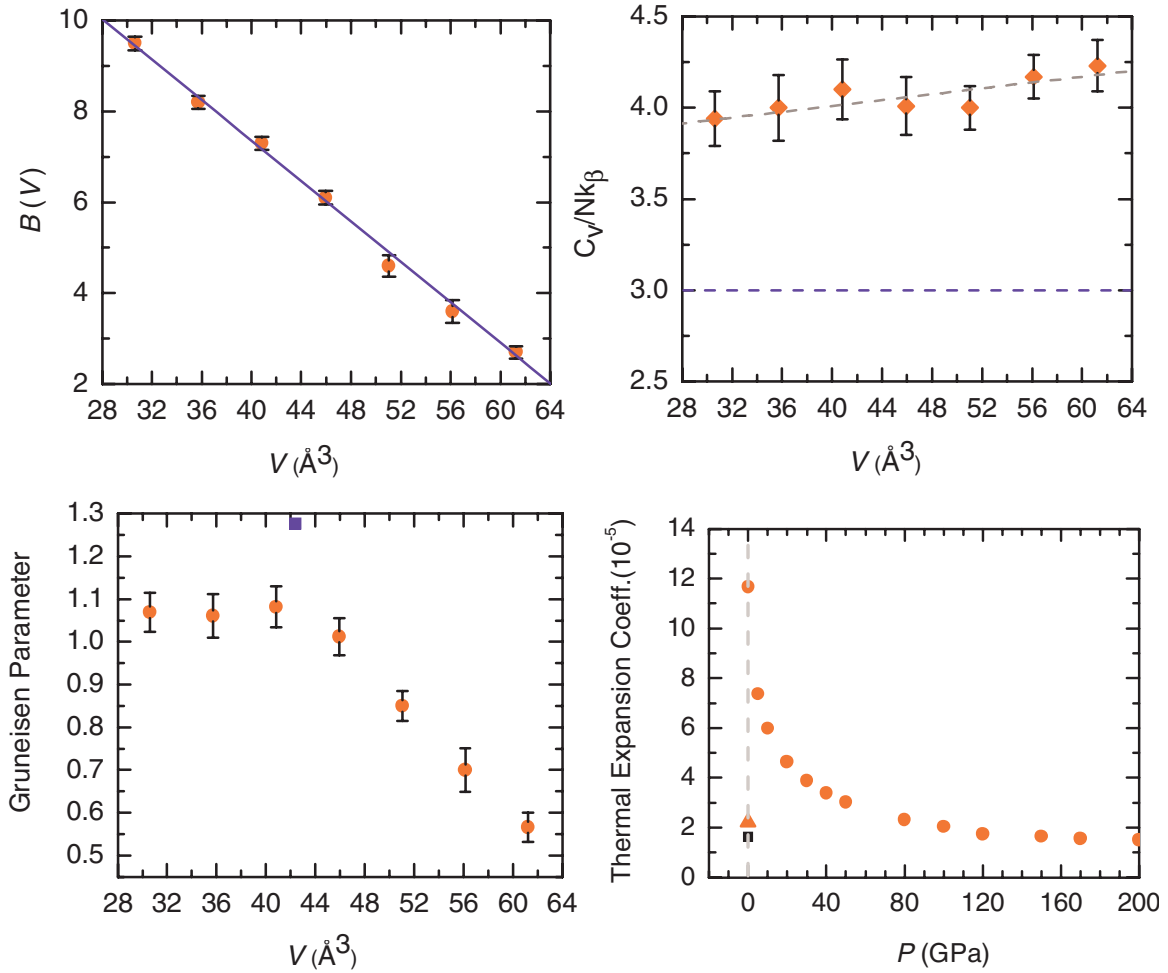


FIG. 2. (Color online) Calculated temperature-average thermal pressure coefficient B (MPa/K), isochoric heat capacity C_V , Grüneisen parameter, and thermal volume expansion coefficient of liquid alumina under compression (circles). Experimental data on corundum are for Grüneisen parameter (Ref. 35) shown by squares and volume thermal expansion data from Ref. 36 (triangles) and Ref. 37 (squares).

isotherm. The solid is about 20% denser than the liquid at ambient pressure, and the density contrast between solid and liquid alumina decreases rapidly with increasing pressure. A consequence is the solid-liquid density crossover, which appears around 90 GPa; i.e., the liquid becomes denser than the solid at pressures above 90 GPa. Such a density crossover, also predicted in silica liquid,¹⁹ is relevant in magma dynamics in Earth's interior.

Pressure and internal energy calculated as a function of volume and temperature can be used to derive various thermodynamic properties of interest. They include the isochoric specific heat capacity C_V , thermodynamic Grüneisen parameter γ , and volume thermal expansion coefficient α defined through the following relations:

$$C_V = \left(\frac{\partial E}{\partial T} \right)_V, \quad (3)$$

$$\gamma = \frac{V}{C_V} \left(\frac{\partial P}{\partial T} \right)_V, \quad (4)$$

$$\alpha = \frac{1}{V} \left(\frac{\partial V}{\partial T} \right)_P. \quad (5)$$

We compute these thermodynamic quantities by assuming that both pressure and energy are linear in temperature for a given volume. The different physical properties are sensitive to compression to different extents (see Fig. 2). The specific heat decreases by about 20% from $4.23 \pm 0.14 Nk_B$ at $V = 61.24$ to $3.94 \pm 0.15 Nk_B$ at $V = 30.63 \text{ \AA}^3$ per formula unit. The Grüneisen parameter increases by 1.5 times over the same volume range, which means that the effect of temperature on pressure actually increases on compression. This opposite behavior to solids for which γ decreases with compression was previously predicted for other liquids.^{18–20} One can attribute the pressure-induced increase in γ to the increase in coordination number.¹⁸ As pressure increases, the thermal expansion coefficient initially decreases rapidly and varies by a factor of 8 over the entire compression range studied.

B. Structural properties

1. Radial distribution functions

Unlike solids, liquids do not possess long-range structural order. The short-range order of liquids is usually probed by radial distribution functions. The partial radial distribution

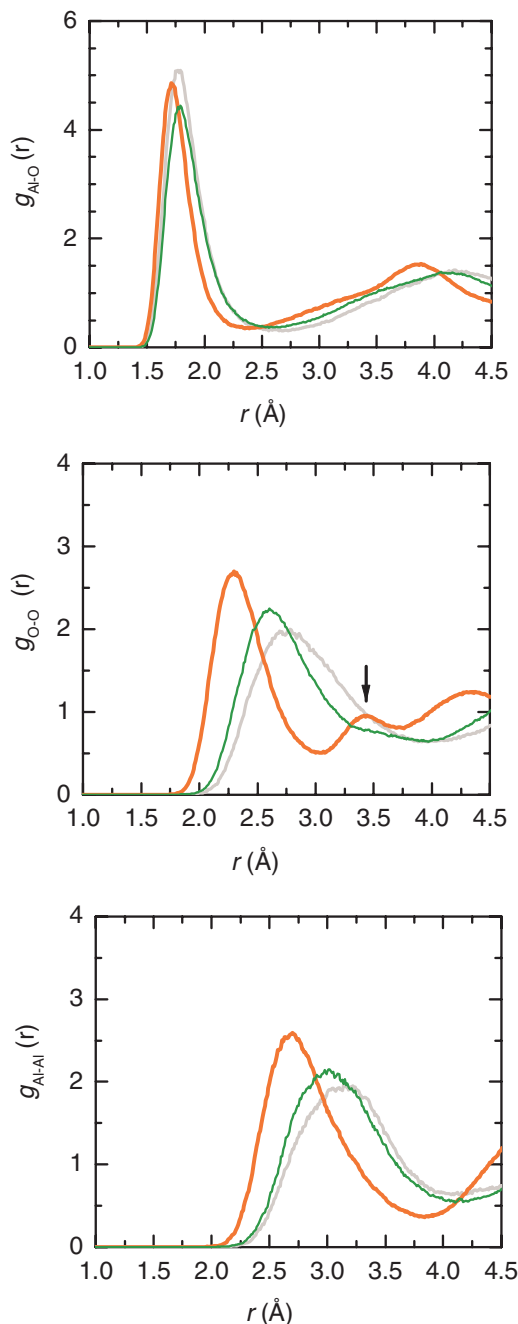


FIG. 3. (Color online) Calculated radial distribution functions at 2.763 (light gray lines), 3.683 (thin olive lines), and 5.524 g/cm^3 (thick red lines) densities at 3000 K. Pressures corresponding to these densities are ~ 2 , 15, and 150 GPa, respectively. The arrow points to the appearance of a new second peak.

function (RDF) $g_{\alpha\beta}(r)$ gives the probability of finding species β at a distance r away from species α relative to that for an ideal gas of the same density. It can be easily calculated by counting the average number $N_{\alpha\beta}$ of β -type ions around an α -type ion inside a spherical shell between r and $r + dr$:³⁸

$$g_{\alpha\beta}(r) = \frac{\langle N_{\alpha\beta}(r, r + \Delta r) \rangle}{4\pi r^2 \Delta r} \frac{V}{N_{\beta}}, \quad (6)$$

where V is the volume of the simulation cell and N_{β} represents the total number of β -type ions.

The calculated radial distribution functions $g_{\text{Al-Al}}(r)$, $g_{\text{O-O}}(r)$, and $g_{\text{Al-O}}(r)$ for $\rho = 2.763$ (–2 GPa), 3.683 (15 GPa), and 5.524 (150 GPa) g/cm^3 at 3000 K are shown in Fig. 3. They were calculated up to half of the simulation cell due to the imposed periodic boundary conditions. The $g_{\text{Al-O}}(r)$ function shows the sharpest first peak and well-defined minimum, and also a broader second peak. This means that Al–O bonding controls the melt structure. The other two functions have relatively broader and shorter peaks, and also the peaks are located at larger distances.

With increasing temperature at a given volume or density, the peaks become shorter, wider, and less symmetric, and the RDF weight at the minimum increases. These changes reflect an increased disorder of melt structure. As the liquid is compressed, the peak positions and amplitudes in $g_{\text{Al-Al}}(r)$ and $g_{\text{O-O}}(r)$ are affected much more than those in $g_{\text{Al-O}}(r)$. The first peak in both like-atom RDFs grows taller and moves to a shorter distance. Even a new second peak appears (indicated with the arrow in Fig. 3) in $g_{\text{O-O}}(r)$ in the close vicinity of the first peak at pressures above 10 GPa—a feature which was previously seen in the simulations of silica and other silicate liquids,^{18,19} suggesting significant rearrangement of O atoms at high pressure. Homopolar bonds (Al–Al and O–O) exist in small proportions as indicated by small overlap of $g_{\text{Al-Al}}(r)$ and $g_{\text{O-O}}(r)$ with the first peak of $g_{\text{Al-O}}(r)$, and the numbers of these bonds increase on compression.

The mode of the first peak in RDF can be taken as the most probable bond length or distance between the corresponding two ions. Thus estimated Al–O, O–O, and Al–Al bond lengths of 1.76, 2.76, and 3.13 Å, respectively, at $\rho = 2.763 \text{ g}/\text{cm}^3$ and 3000 K are in excellent agreement with the experimental data. The latest neutron diffraction study for $\rho = 2.81 \text{ g}/\text{cm}^3$ has found a first Al–O peak at $1.76 \pm 0.1 \text{ Å}$ and a second O–O peak around 2.8 Å¹⁷. However, in an x-ray diffraction experiment the Al–O, O–O, and Al–Al bond lengths were estimated to be 1.76, 3.08, and 4.25 Å, respectively.¹¹ Note that the peak assignment in experiments is dependent on how the peaks are modeled and interpreted. Previous classical molecular dynamics results are in good agreement with our first-principles results (see Table II). All bond distances decrease with increasing pressure (Fig. 4), with the Al–O distance showing much smaller variations ($\sim 4\%$) compared to O–O and Al–Al distances ($\sim 15\%$) over the entire pressure regime studied. This suggests that O–O and Al–Al correlations play an increasingly important role in the densification of Al_2O_3 liquid on compression.

2. Coordination numbers

All partial radial distribution functions $g_{\alpha\beta}(r)$'s changing with temperature and compression imply that the coordination environments (which represent the local packing of atoms) are also sensitive to both temperature and pressure. There are four types of coordination environments, which include like-atoms (Al–Al and O–O) and unlike-atoms (Al–O and O–Al) coordination. The mean coordination number $n_{\alpha\beta}$ can be calculated using

$$n_{\alpha\beta}(R_{\min}) = \frac{4\pi N_{\beta}}{V} \int_0^{R_{\min}} g_{\alpha\beta}(r) r^2 dr, \quad (7)$$

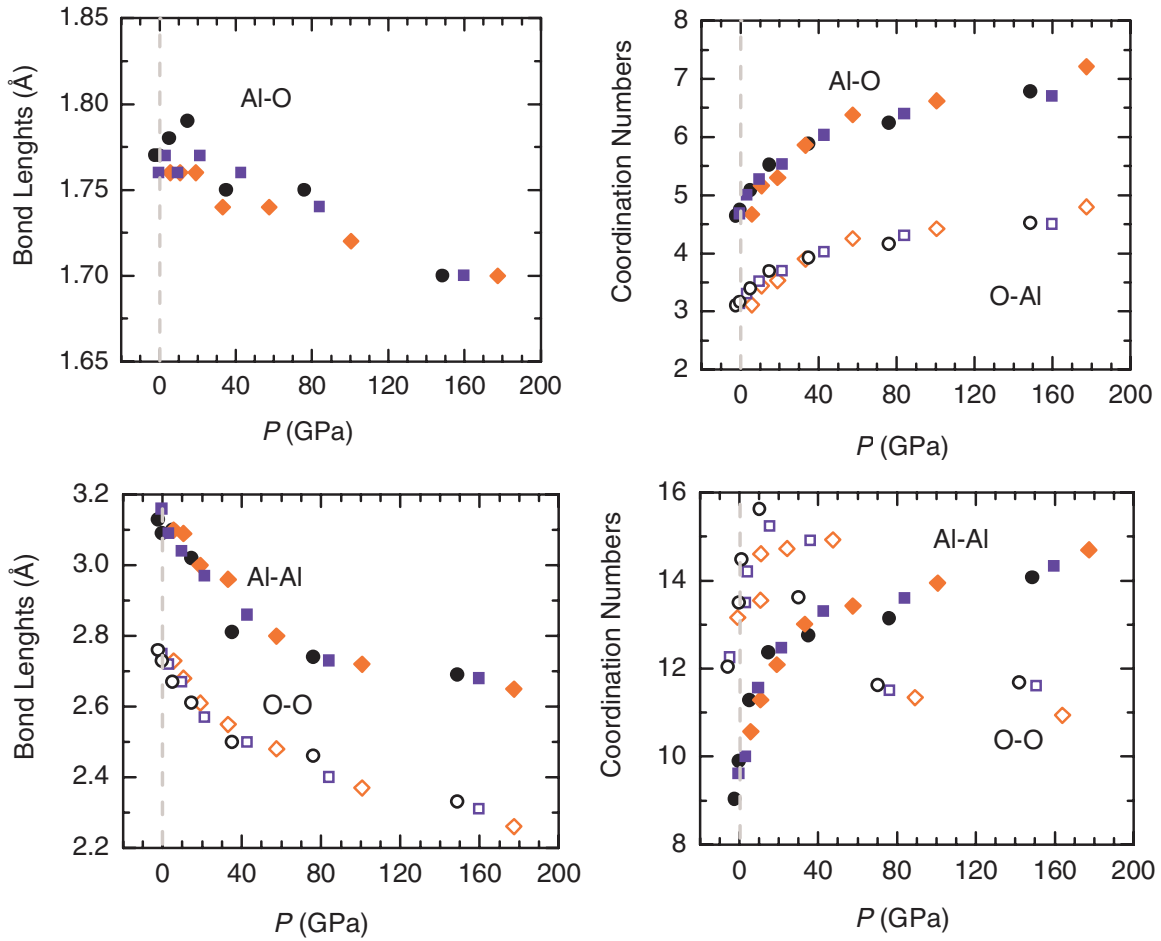


FIG. 4. (Color online) Pressure variations of the calculated average bond distances and coordination numbers for liquid alumina at 3000 (circles), 4000 (squares), and 6000 K (diamonds). Gray vertical lines mark the zero pressure.

where R_{\min} is the position of the first minimum of the corresponding radial distribution function (see Table II). At 0 GPa and 3000 K, the calculated mean Al–O coordination number is 5.2 which lies within the experimental range of 4.2 to 5.6 (Refs. 11–13). Our result also compares well with previous classical MD results (see Table II). As shown in Fig. 4,

the mean coordination numbers for all types Al–O, O–Al, Al–Al, and O–O increase considerably as pressure increases, suggesting increased packing of atoms on compression. The Al–O and O–Al coordination numbers increase from 5.2 and 3.4, respectively, at 0 GPa and 3000 K, to 6.8 and 4.5, respectively, at 150 GPa and 3000 K. In contrast, the effects

TABLE II. Calculated positions of the first peak ($r_{\alpha\beta}$), and the first minimum (R_{\min}) of different radial distribution functions together with coordination numbers ($n_{\alpha\beta}$) for three selected densities at 3000, 4000, and 6000 K. All distances are in Å and densities are in g/cm^3 .

| | | $\rho = 2.763$ | $\rho = 3.683$ | $\rho = 5.524$ | Previous results |
|-------|--------------------|------------------|------------------|------------------|---|
| Al–O | $r_{\text{Al–O}}$ | 1.77, 1.76, 1.77 | 1.79, 1.77, 1.74 | 1.70, 1.70, 1.70 | $r_{\text{Al–O}}$: 1.78, ^a 1.75, ^b 1.75 ^c |
| | R_{\min} | 2.65, 2.69, 2.70 | 2.59, 2.59, 2.69 | 2.41, 2.49, 2.51 | $r_{\text{Al–Al}}$: 3.20, ^c 3.15 ^b |
| | $n_{\text{Al–O}}$ | 4.64, 4.68, 4.67 | 5.52, 5.53, 5.86 | 6.78, 6.75, 7.21 | $r_{\text{O–O}}$: 2.79, ^c 2.75 ^b |
| Al–Al | $r_{\text{Al–Al}}$ | 3.13, 3.16, 3.10 | 3.02, 2.97, 2.96 | 2.69, 2.68, 2.65 | $n_{\text{Al–O}}$: 4.41, ^a 4.1, ^b 3.91 ^c |
| | R_{\min} | 4.10, 4.19, 4.35 | 4.13, 4.15, 4.23 | 3.78, 3.83, 3.84 | $n_{\text{Al–Al}}$: 7.46, ^c 8.24 ^b |
| | $n_{\text{Al–Al}}$ | 9.0, 9.61, 10.6 | 12.4, 12.5, 13.0 | 14.1, 14.3, 14.7 | $n_{\text{O–O}}$: 6.87, ^c 8.84 ^b |
| O–O | $r_{\text{O–O}}$ | 2.76, 2.75, 2.73 | 2.61, 2.57, 2.55 | 2.33, 2.31, 2.26 | $n_{\text{O–Al}}$: 2.79, ^c 2.72 ^b |
| | R_{\min} | 3.93, 3.96, 4.07 | 3.95, 3.90, 3.84 | 3.05, 3.04, 2.99 | |
| | $n_{\text{O–O}}$ | 12.0, 12.3, 13.2 | 15.6, 15.2, 14.7 | 11.7, 11.6, 10.9 | |
| O–Al | $n_{\text{O–Al}}$ | 3.1, 3.12, 3.1 | 3.69, 3.69, 3.90 | 4.52, 4.50, 4.80 | |

^aReference 1: For $\rho = 2.81 \text{ g}/\text{cm}^3$ at 2600 K.

^bReference 7: For $\rho = 3.175 \text{ g}/\text{cm}^3$ at 2200 K.

^cReference 8: For $\rho = 2.65 \text{ g}/\text{cm}^3$ at 3500 K.

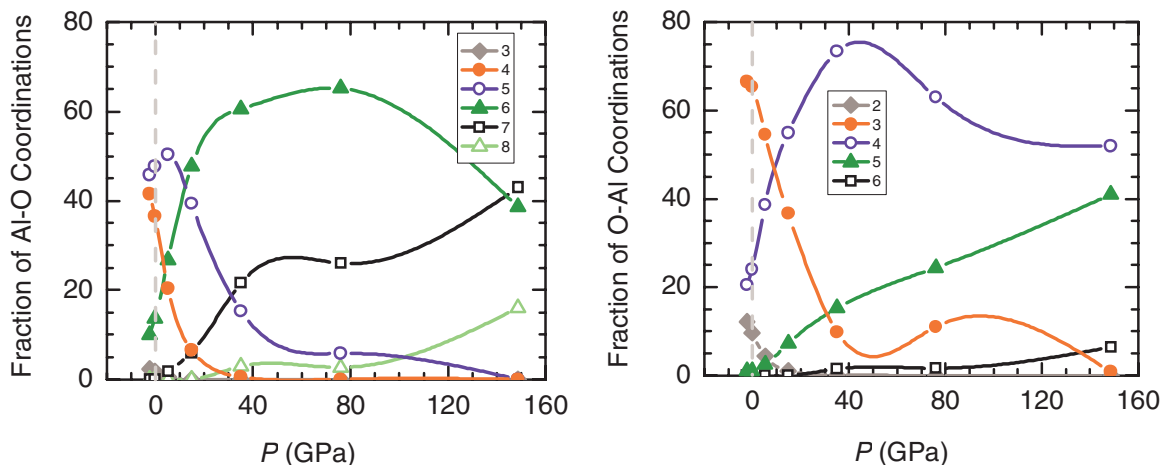


FIG. 5. (Color online) Abundances (%) of different coordination species (zC_{AlO} and zC_{OAl}) in liquid Al_2O_3 as a function of pressure at 3000 K.

of temperature on coordination are relatively small at a fixed density because the RDF peaks become broader and shorter to similar extents.

The Al and O coordination environments consist of various species whose abundances change with temperature and pressure. Temperature shows a general trend that coordination distribution becomes broader with the appearance of new species (both low and high coordination) but without significantly affecting the mean coordination numbers on isochoric heating. On the other hand, pressure tends to systematically shift coordination distribution to high value with appearance of high-coordination species at the cost of low-coordination species. Pressure variations of various Al–O and O–Al coordination species at 3000 K are shown in Fig. 5. At zero pressure, the four-, five- and sixfold Al–O coordination species are present in significant amounts (36, 48, and 14%). As the liquid is compressed, the tetrahedral abundance decreases very fast whereas the pentahedral abundance initially increases and then decreases beyond 10 GPa. As a consequence, the abundance of sixfold coordination (octahedral) species gradually increases and also high-coordination species including seven- and eightfold coordination species appear at high pressure. Their respective values are 37, 43, and 16% at 150 GPa and 3000 K. On the other hand, the O–Al coordination changes from being dominated by three- and fourfold species (65 and 24%) at the ambient pressure to being dominated by four- and fivefold species (52 and 41%) at 150 GPa and 3000 K pressure.

A high degree of Al and O coordination means that Al_2O_3 liquid is highly networked. To further explore the connectivity, we examine the distribution of the quantity zAl^n , which is similar to the widely used quantity Q^n defined for fourfold Si–O coordination ($Z = 4$) in silicates. Here, n is the number of bridging oxygen atoms (an oxygen atom which is also bonded to one or more Al atoms) attached to an Al atom under consideration, which can be in any coordination state in our case (see Table III). The calculated distribution consists of a mixture of different species with zAl^4 , zAl^5 , and zAl^6 dominating at low pressure. The absence of zAl^0 and zAl^1 species means that the Al–Al network is complete. As compression increases, the distribution shows increased abundances of higher-order species, zAl^6 , zAl^7 , and zAl^8 species together counting for 98%. The preponderance of higher-order species in compressed liquids is consistent with the increased ${}_4C_{OAl}$ and ${}_5C_{OAl}$ abundances (see Table IV).

The high degree of structural packing is reflected by relatively high mean values of Al–Al and O–O coordination. The Al–Al coordination number increases monotonically from 11.4 to 14.6 between 0 to 150 GPa at 3000 K. On the other hand, the mean O–O coordination number falls significantly after 10 GPa and then again gradually increases with pressure reaching 11.5 at 150 GPa. The predicted abrupt change in the O–O coordination can be attributed to the pressure-induced pushing of the first peak and minimum in $g_{O-O}(r)$ to smaller distances and also to the eventual appearance of a new second peak. Our results show that both Al–Al and O–O coordination show a

TABLE III. Percentage abundances of various zAl/Si^n species of liquid alumina and silica.

| T (K), P (GPa) | zAl^3 | zAl^4 | zAl^5 | zAl^6 | zAl^7 | zAl^8 |
|--------------------|---------|---------|---------|---------|---------|---------|
| 3000, 5 | 0.31 | 16 | 49 | 32 | 2.09 | 0.09 |
| Silica | 0.98 | 97 | 1.6 | 0.01 | 0.00 | 0.00 |
| 4000, 9.6 | 0.49 | 16 | 45 | 33 | 4.5 | 0.19 |
| 6000, 19 | 1.9 | 16 | 40 | 33 | 8.4 | 0.83 |
| 3000, 35 | 0.00 | 0.48 | 13 | 60 | 24 | 3.4 |
| 3000, 150 | 0.00 | 0.00 | 0.69 | 36 | 45 | 18 |

TABLE IV. Abundances of various Al–O coordination species (denoted as ${}_Z C_{\text{AlO}}$ and ${}_Z C_{\text{OAl}}$) of alumina liquid compared with Si–O coordination in silica liquid. Here, Z represents the coordination number.

| T (K), P (GPa) | ${}_3 C_{\text{AlO}}$ | ${}_4 C_{\text{AlO}}$ | ${}_5 C_{\text{AlO}}$ | ${}_6 C_{\text{AlO}}$ | ${}_7 C_{\text{AlO}}$ | ${}_2 C_{\text{OAl}}$ | ${}_3 C_{\text{OAl}}$ | ${}_4 C_{\text{OAl}}$ | ${}_5 C_{\text{OAl}}$ |
|--------------------|-----------------------|-----------------------|-----------------------|-----------------------|-----------------------|-----------------------|-----------------------|-----------------------|-----------------------|
| 3000, 5 | 0.33 | 16 | 49 | 32 | 2.90 | 3.0 | 51 | 42 | 3.8 |
| Silica | 0.44 | 98 | 1.6 | 0.02 | 0.00 | 99 | 0.76 | 0.00 | 0.00 |
| 4000, 9.6 | 0.54 | 16 | 45 | 33 | 4.5 | 4.2 | 47 | 44 | 5.4 |
| 6000, 19 | 1.9 | 16 | 40 | 33 | 8.4 | 6.2 | 42 | 43 | 8.7 |
| 3000, 35 | 0.00 | 0.47 | 13 | 60 | 24 | 0.06 | 8.7 | 72 | 17 |
| 3000, 150 | 0.00 | 0.00 | 0.69 | 36 | 45 | 0.00 | 0.08 | 49 | 45 |

wide variety with 12-fold and higher species existing in large amounts (50 to 95% in total) at the highest pressure studied.

Comparison between Al_2O_3 and SiO_2 liquids allows us to understand the effects of Al_2O_3 and SiO_2 components on the properties of silicate melts. The calculated Al–O RDF shows a shorter and broader first peak located at larger distance, compared to the first peak in the Si–O RDF. This is consistent with larger effective size of the Al ion. Not only are Al–O bonds relatively long, they are also relatively weak and are hence broken at much higher rates than Si–O bonds (see Table V). These differences mean that the two liquids show significant differences in their structures. Al_2O_3 liquid shows higher coordination and a richer set of coordination species than SiO_2 liquid. Both liquids form complete networks, which are of different types. SiO_2 liquid essentially represents a nearly pure tetrahedral network (98% four-oxygen-coordinated Si and 99% bridging oxygen, i.e., two-silicon-coordinated O).¹⁹ On the other hand, Al_2O_3 liquid consists of a mixture of different Al–O coordination polyhedra in significant proportions; almost half of the Al atoms are fivefold coordinated with oxygen, the other half showing four- and sixfold coordination. Consistently, O–Al coordination is dominated by three- and fourfold species with only about 3% bridging oxygen. The bond activities also control transport properties including diffusion and viscosity coefficients. Since new Al–O bonds are formed at a higher rate than new Si–O bonds, Al_2O_3 liquid should show faster dynamics than silica liquid (see Table V).

TABLE V. Al–O bond parameters at different conditions. Here, α_B is the rate of bond breakings (per picosecond), τ_B is the mean bond lifetime (in femtoseconds) defined as N_B/α_B , where N_B is the mean number of Al–O bonds in the simulation cell (i.e., 48 times mean coordination number), and α_T represents the fraction of the bond events, which result in the formation of new bonds and thus cause the transfer of oxygen from one coordination shell to another. Si–O bond parameters for silica liquid are also given.

| T (K), P (GPa) | α_B | τ_B | α_T |
|--------------------|------------|----------|------------|
| 3000, 5 | 590 | 430 | 0.21 |
| Silica | 19 | 5050 | 0.16 |
| 4000, 9.6 | 835 | 300 | 0.24 |
| 6000, 19 | 1340 | 187 | 0.24 |
| 3000, 35 | 780 | 422 | 0.08 |
| 3000, 150 | 830 | 399 | 0.04 |

3. Bond-angle distributions

We now describe the melt structure in terms of bond-angle distributions. Two bond angles are of interest: The O–Al–O bond-angle contains the intrapolyhedral information whereas the Al–O–Al bond tells us about interpolyhedral connectivity. Figure 6 shows the bond-angle distributions using R_{min} in $g_{\text{Al-O}}(r)$ calculated for $\rho = 2.763, 3.683, \text{ and } 5.524 \text{ g/cm}^3$ at 3000 K. The O–Al–O bond-angle distribution has a broad peak between 92° and 121° , with a large dispersion extending to 180° . We separate the bond-angle distribution into three components corresponding to tetrahedra, pentahedra, and octahedra, which show maxima around 105° , 85° , and 75° (second maximum peak at 160°), respectively. Note that the O–Al–O bond-angle for ideal tetrahedron is 109.47° , and for pentahedron and octahedron the possible values are 90° and 180° . The bond-angle analysis also supports the prediction that the liquid state consists of the distorted tetrahedral, pentahedral, and octahedral units. These polyhedral units are linked to form a network with Al–O–Al angle peaked at 94° with broad dispersion towards the larger angles. On compression, the major peak of O–Al–O distribution shifts towards lower angles and becomes sharper. An extra peak starts to develop around 135° . This bimodal distribution is consistent with the melt structure dominated by octahedra and high-coordination polyhedra. Similarly, the Al–O–Al bond-angle distribution becomes bimodal with the first peak becoming sharper with a shoulder appearing at the high angle side as the liquid is compressed.

IV. SUMMARY

Using first-principles molecular dynamics simulations, the thermodynamical and structural properties of liquid Al_2O_3 were probed extensively. The density contrast between liquid and solid alumina decreases rapidly with compression and around 90 GPa the density crossover occurs, i.e., liquid becomes denser than solid. This density crossover is expected to result in a maximum of the melting temperature under pressure. The calculated P - V - T results were successfully described with the Mie–Grüneisen form of the equation of state. The constant volume specific heat coefficient of liquid alumina is much higher than what is expected from the classical theory of Dulong–Pettit; i.e., liquid alumina can hold much higher heat than the Dulong and Pettit liquid for a given temperature rise. With compression the constant volume heat capacity decreases but it always remains above the classical value. The liquid Grüneisen parameter varies unusually with compression, i.e.,

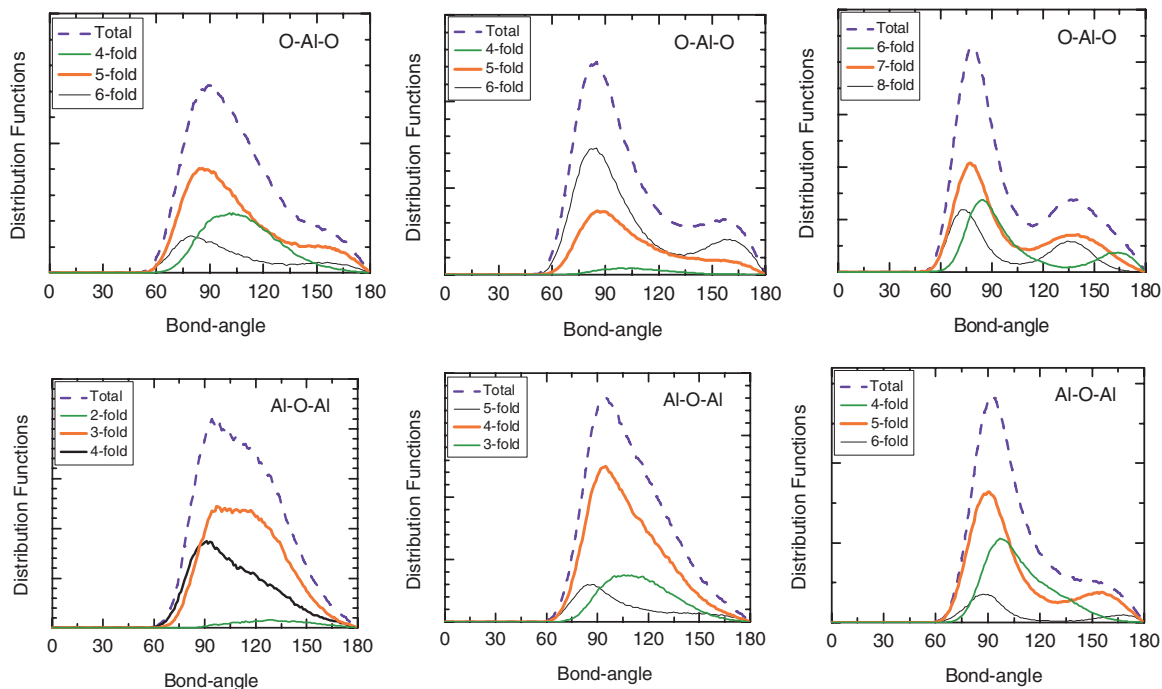


FIG. 6. (Color online) Calculated bond-angle distribution functions (in arbitrary units) for densities, $\rho = 2.763$ (left column), 3.683 (middle column), and 5.524 g/cm^3 (right column) at 3000 K .

unlike in solids, it increases with compression by a factor of 1.5 over the studied density range. The linear thermal expansion coefficient initially decreases sharply with pressure and it changes by a factor of 8 over the entire pressure range. The predicted behavior of various properties can be attributed to the continuous structural change of liquid with compression unlike in solids where the structural changes are always discontinuous. We find that liquid alumina shows a rich variety of structural features (which are lacking in a solid), which are defined in terms of bond length and angle distributions, and coordination environments. The liquid alumina is highly

networked. The mean Al–O and O–Al coordination numbers increase from 5.2 and 3.4, respectively, at 0 GPa and 3000 K, to 6.8 and 4.5, respectively, at 150 GPa and 3000 K. Coordination environments consist of various species whose abundances change as the liquid is compressed.

ACKNOWLEDGMENTS

Computing facility was provided by Computer Division at Bhabha Atomic Research Centre. BBK acknowledges support from NSF (EAR-0809489).

*ashokverma77@gmail.com

¹P. Vashishta, R. K. Kalia, A. Nakano, and J. P. Rino, *J. Appl. Phys.* **103**, 083504 (2008).

²R. E. Cohen, *Geophys. Res. Lett.* **14**, 37 (1987).

³W. Duan, R. M. Wentzcovitch, and K. T. Thomson, *Phys. Rev. B* **57**, 10363 (1997).

⁴B. B. Karki, L. Stixrude, and R. M. Wentzcovitch, *Rev. Geophys.* **39**, 507 (2001).

⁵A. R. Oganov and S. Ono, *Proc. Natl. Acad. Sci. USA* **102**, 10828 (2005).

⁶M. Hemmati, M. Wilson, and P. A. Madden, *J. Phys. Chem. B* **103**, 4023 (1999).

⁷G. Gutierrez, A. B. Belonoshko, R. Ahuja, and B. Johansson, *Phys. Rev. E* **61**, 2723 (2000).

⁸V. V. Hoang, *Phys. Rev. B* **70**, 134204 (2004).

⁹P. K. Hung, N. T. Nhan, and L. T. Vinh, *Modell. Simul. Mater. Sci. Eng.* **17**, 025003 (2009).

¹⁰S. Jahn and P. A. Madden, *J. Non-Cryst. Solids* **353**, 3500 (2007).

¹¹S. Ansell, S. Krishnan, J. K. R. Weber, J. R. Felten, P. C. Nordine, M. A. Beno, D. L. Price, and M.-L. Saboungi, *Phys. Rev. Lett.* **78**, 464 (1997).

¹²C. Landron, L. Henet, T. E. Jenkins, G. N. Creaves, J. P. Coutures, and A. K. Soper, *Phys. Rev. Lett.* **86**, 4839 (2001).

¹³Y. Waseda, K. Sugiyama, J. M. Toguri, and Z. Naturforsch., *A. Phys. Sci.* **50**, 770 (1995).

¹⁴J. P. Coutures, D. Massiot, C. Bessada, P. Echegut, J. C. Rifflet, and F. Taulelle, *C. R. Acad. Sci.* **310**, 1041 (1990).

¹⁵D. Massiot, F. Taulelle, and J. P. Coutures, *Colloq. Phys. C5*, 425 (1990).

¹⁶L. Vocadlo, D. Alfe, M. J. Gillan, I. G. Wood, J. P. Brodholt, and G. D. Price, *Nature* **424**, 536 (2003).

¹⁷N. Jakse and A. Pasturel, *Phys. Rev. Lett.* **91**, 195501 (2003).

¹⁸L. Stixrude and B. B. Karki, *Science* **301**, 297 (2005).

¹⁹B. B. Karki, D. Bhattarai, and L. Stixrude, *Phys. Rev. B* **76**, 104205 (2007).

- ²⁰N. P. de Koker, L. Stixrude, and B. B. Karki, *Geochim. Cosmochim. Acta* **72**, 1427 (2008).
- ²¹G. Kresse and J. Hafner, *J. Phys.: Condens. Matter* **6**, 8245 (1994).
- ²²G. Kresse and J. Furthmuller, *Comput. Mater. Sci.* **6**, 15 (1996).
- ²³P. E. Blöchl, *Phys. Rev. B* **50**, 17953 (1994).
- ²⁴S. Nosè, *Mol. Phys.* **52**, 255 (1989).
- ²⁵H. Flyvege and H. G. Petersen, *J. Chem. Phys.* **91**, 461 (1989).
- ²⁶P. Paradis, T. Ishikawa, Y. Saita, and S. Yoda, *Jpn. J. Appl. Phys.* **43**, 1496 (2004).
- ²⁷B. Glorieux, F. Millot, J. C. Rifflet, and J. P. Coutures, *Int. J. Thermophys.* **20**, 1085 (1999).
- ²⁸J.-P. Coutures, J.-C. Rifflet, P. Florian, and D. Massiot, *Rev. Int. Hautes Temp. Refract.* **29**, 1085 (1994).
- ²⁹E. E. Shpil'rain, K. A. Yakinovich, and F. Tsitsarkin, *High Temp.—High Pressures* **191**, 2 (1973).
- ³⁰H. d'Amour, D. Schiferi, W. Denner, H. Schulz, and W. B. Holzapfel, *J. Appl. Phys.* **49**, 4411 (1978).
- ³¹P. Richet, J. Xu, and H. Mao, *Phys. Chem. Miner.* **16**, 207 (1988).
- ³²S. Sandro, P. A. Madden, and M. Wilson, *Phys. Rev. B* **74**, 024112 (2006).
- ³³G. Fiquet, P. Richet, and G. Montagnac, *Phys. Chem. Miner.* **27**, 103 (1986).
- ³⁴S. P. Marsh, in *Minerals and Compounds*, edited by S. P. Marsh (University of California Press, Berkeley, 1980), p. 260.
- ³⁵A. Kirfel and K. Eichhorn, *Acta Cryst. A* **46**, 271 (1990).
- ³⁶E. Schreiber and O. L. Anderson, *J. Am. Ceram. Soc.* **49**, 184 (1966).
- ³⁷E. S. Zouboulis and M. Grimditch, *J. Appl. Phys.* **70**, 772 (1991).
- ³⁸P. Vashishta, R. K. Kalia, J. P. Rino, and I. Ebbsjo, *Phys. Rev. B* **41**, 12197 (1990).